Progress In Electromagnetics Research M, Vol. 73, 173–181, 2018

A Modified Planar Inverted-F Antenna with Triple-Band for Wi-Fi and LTE Applications

Yun Jing Zhang, Dan Wang, Li Zhang, and Mei Song Tong*

Abstract—A compact planar double inverted-F antenna (IFA) is proposed in this work. The antenna, composed of a shared short arm and two L-shaped open arms, has three operating bands, 1.7–1.9 GHz, 2.25–2.48 GHz and 5.33–5.8 GHz for Wi-Fi and LTE applications. It has the length of 80 mm, width of 23 mm and height of 1.6 mm. Near omnidirectional coverage of radiation patterns in x-y and x-z plane, are realized with peak gain of 3.3 dBi, 2.1 dBi and 4.1 dBi at 1.8 GHz, 2.4 GHz and 5.5 GHz, respectively. Based on reflection coefficients with different dimensions and current distributions, the functions of arms and via holes are analyzed in detail, which provide a useful guidance for design of multiband PIFA antennas.

1. INTRODUCTION

Wireless communication technology has been developed rapidly and played an important role in our works and lives [1–4]. Wireless fidelity (Wi-Fi) is a superset of the IEEE 802.11 standards for wireless communications at the frequencies of 2.4 GHz (2.4–2.483 GHz) and 5.0 GHz (5.15–5.35 GHz and 5.47–5.825 GHz) and was designated to industrial, scientific, and medical (ISM) bands [5]. Long Term Evolution (LTE) is also a standard for wireless communication which is based on GSM/EDGE and UMTS/HDSPA network using mobile phones or mobile devices and has different bands for different countries [6]. Among all Wi-Fi and LTE communication components, antennas play an irreplaceable role. As the size of wireless devices becomes smaller and smaller, designing a compact, low-cost, and multiband antenna is very challenging.

Planar monopole antennas [7–9] are considered as good candidates for Wi-Fi and LTE systems because of their low profile, light weight, easy fabrication, and multiband operation. A triple-arm antenna is adopted in [7], and it naturally has three bands, but its gain is small, and radiation patterns are not measured yet. In [9], the monopole antenna employs a T-shape technique and can achieve a dual-band property. However, a shorted parasitic element used to enhance its bandwidth increases the complexity of structure, and the large ground plane also limits its application [10, 11]. To isolate the impact of the ground plane, a multiband resonator antenna is designed in [12]. The thick substrate, however, leads to a high profile. To overcome the shortcomings of above antennas, the inverted-F antenna (IFA) is proposed. In [13], a multi-branch IFA antenna was designed with a multiband feature and relatively high gain. However, the large ground and complex strip arrangement have greatly restricted its applications. A small IFA for Wi-Fi USB applications was proposed in [14], and it has two narrow bands with low gain. Furthermore, a planar hexa-band IFA was proposed and owns a better bandwidth characteristic [15], but −6 dB rather than −10 dB is used as a reference of reflection coefficient for defining the bandwidth. Besides, the antenna has a complicated branch. To simplify the structure of the antenna, a multiband IFA was presented in [16], and it has three narrow bands. The antenna was etched on an expensive 0.127-mm RT5800 substrate, and it is inconvenient to

Received 20 August 2018, Accepted 12 September 2018, Scheduled 26 September 2018
* Corresponding author: Mei Song Tong (mstong@tongji.edu.cn).
The authors are with the Department of Electronic Science and Technology, Tongji University, China.

be integrated with printed circuit boards (PCBs). More recently, a stacked IFA with two shorted strips was proposed for the application of tablet devices [17]. Nevertheless, the cubic structure may not be desirable anymore as the tablet devices have become thinner. The planar IFA (PIFA) was proposed which lowers the profile of the IFA [18]. Then, a dual-frequency PIFA was designed in [19, 20], and its slotted patch or ground can produce two different frequency bands [21]. A miniaturized PIFA [22] with a four-element diversity was designed by employing a meandered technique [23, 24], but just one band (2.4 GHz) was achieved.

Although various efforts have been made, the performance and structure of antennas have never been perfect, and a further improvement is always needed. In this work, we propose a double PIFA antenna. Compared with those IFAs and PIFAs mentioned above, it presents some advantages, such as a small-size ground, simplified structure, and high gain. In addition, an FR4 substrate is used to reduce the manufacturing cost and be integrated with PCBs. The connected patch between the first open arm and feed port is tilted so that the gain can be enhanced. The good performance of the antenna is verified with the consistence between simulated and measured results. It is noticed that the analyses of the functions of arms and via holes provide the guidance of the PIFA design.

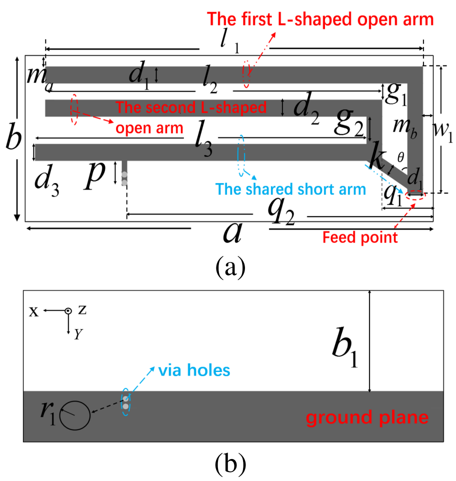

Figure 1. Geometry of the proposed inverted-F antenna. (a) Top view. (b) Bottom view.

2. ANTENNA DESIGN

The proposed antenna is shown in Fig. 1, and its front and back views are sketched in Fig. 1(a) and Fig. 1(b), respectively. The antenna has two L-shaped open arms and a shared short arm. The ground plane covers part of the bottom side, and the shared short arm is connected by a shorted stub with two via holes. The two L-shaped open arms share the same short arm as well as the ground plane, yielding a double inverted-F structure. This antenna is etched on a cheap RF4 substrate with a relative permittivity of 4.4, thickness of 1.6 mm, and dielectric loss tangent of 0.02. The entire antenna has a length of 80 mm and width of 45 mm. Note that only 23 mm in the width is used as the antenna part, meaning that the antenna can be etched and integrated on a PCB diminutively and conveniently. The optimized dimensions using HFSS software are listed in Table 1.

Table 1. Dimensions of the proposed antenna (unit: mm).

a	b	b_1	l_1	l_2	l_3	d_1	d_2	d_3	q_1
80	45	20	74	66	65	3	3	3	10
w_1	g_1	g_2	r_1	m_a	m_b	p	θ°	k	q_2
23	3	5	0.5	2	2	4	58	1	60

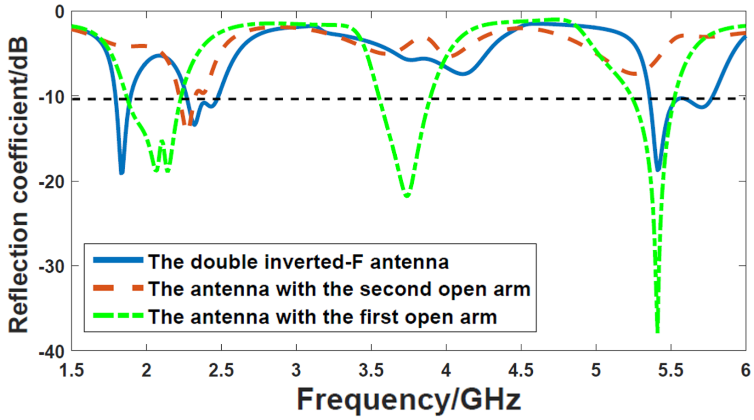

Figure 2. Reflection coefficients of the antenna with different arms combined.

The structure of the proposed antenna can be divided into two IFAs, which consist of the first L-shaped open arm and second L-shaped open arm, respectively. In order to clarify the influence of the arms, we separately investigate each of the two arms. Fig. 2 shows the reflection coefficients of the antenna with different arms combined. Dashed and dot-dashed lines represent the reflection coefficients of the first IFA and second IFA, respectively. It can be seen that the antenna with one of the two L-shape arms presents a resonant frequency lower than that of the antenna with both L-shape arms in the lower band (2.4- GHz). This means that the coupling of the two L-shape arms increases the resonant frequency in the lower band. The antenna with the first L-shape arm has a resonant frequency of 5.4 GHz, but the frequency disappears for the antenna with the second L-shape arm. Therefore, the resonant frequency of 5.8 GHz of the antenna (with two L-shape arms) in the upper band is purely produced by the coupling of two L-shape arms. Additionally, the resonant frequency of 1.82 GHz is also generated by the coupling. Solid line in Fig. 2 shows that the antenna has three frequency bands, which range from 1.7 to 1.9 GHz, 2.25 to 2.48 GHz, and 5.33 to 5.8 GHz, respectively.

3. OPTIMIZATION AND ANALYSIS

To achieve the best design for the proposed antenna, we analyze and optimize several parameters in the structure. Fig. 3 shows simulated results with varying parameters. As shown in Figs. 3(a) (b) and (c), l_1 has a main influence on the frequency around 1.82 GHz and the upper band (5.5-GHz). As l_1 increases, the resonant frequency decreases. On the other hand, l_2 and w_1 mainly determine the lower band (2.4-GHz) and upper band (5.5-GHz), respectively. This can be understood by that the length of the coupling between the two open arms mainly decides the lower band, while the distance between the two open arms in the coupling mainly contributes to the upper band.

Figure 3(d) shows the reflection coefficients with different q_1 values. The dimension q_1 changes both the distance and length of the coupling of the two open arms, so it has an influence on both lower and upper bands. Because θ in Fig. 1(a) is an acute angle, q_1 changes the length more than the distance of the coupling. Consequently, q_1 mainly determines the lower frequency band. Fig. 3(e) illustrates the relation between reflection coefficients and parameter q_2. With the change of q_2, all of these bandwidths are changed except the low band from 1.7 to 1.9 GHz, because the distance between the y axis and via holes has an influence on the overall configuration. The reason that the lowest band keeps unchanged is that this band mainly depends on the gap between the ground plane and the shared short arm. In Fig. 3(f), the refection coefficients of the antenna with one via hole and two via holes are exhibited, respectively. It is observed that adding another via hole can expand the frequency bands, which can be understood that the addition of a via hole increases its current density and weakens the capacitance of the open arms.

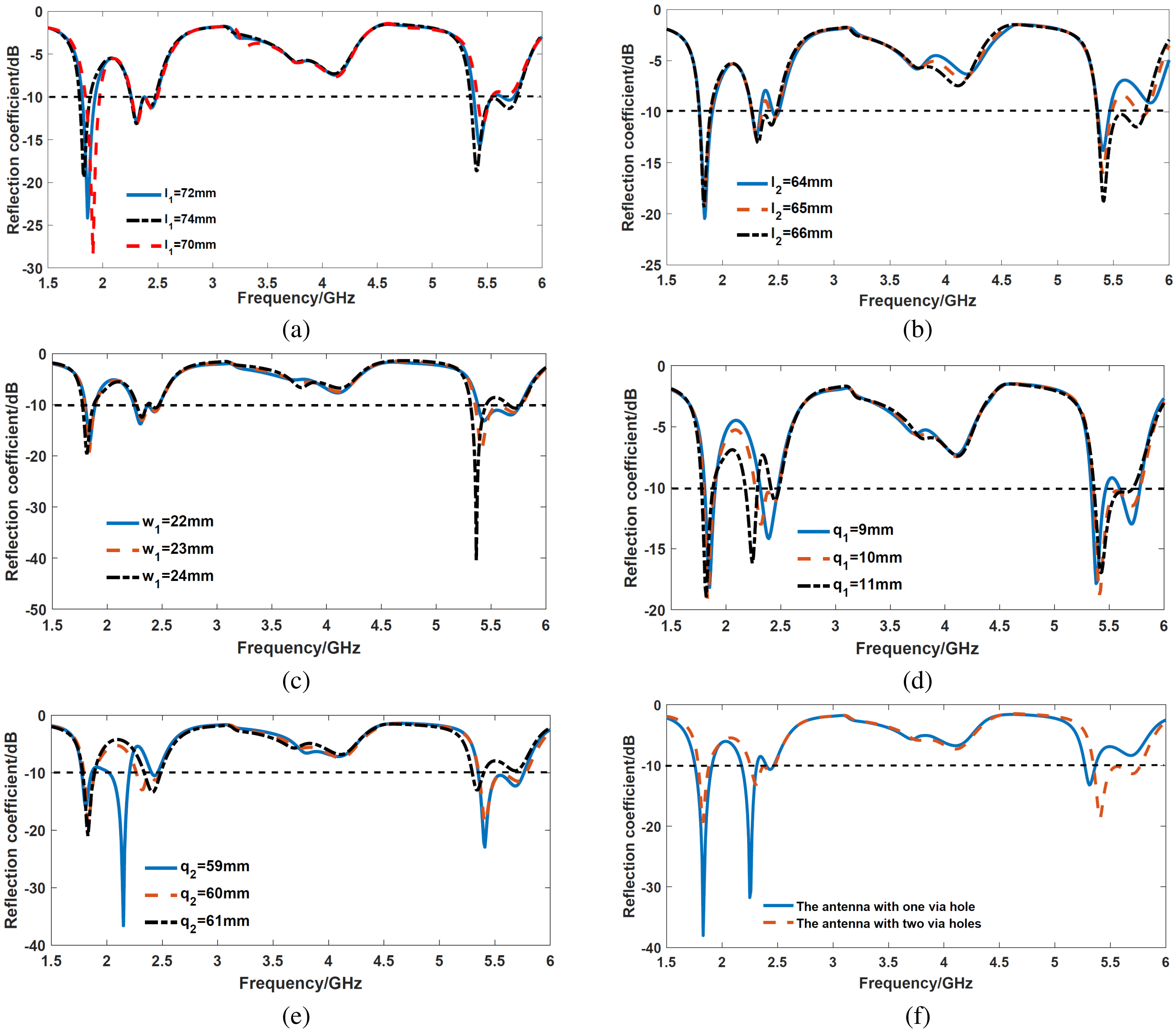

Figure 3. Reflection coefficients of the proposed antenna with different dimensions (mm) or via holes. (a) l_1 is chosen as 70, 72, and 74, respectively. (b) l_2 is chosen as 64, 65, and 66, respectively. (c) w_1 is chosen as 22, 23, and 24, respectively. (d) q_1 is chosen as 9, 10, and 11, respectively. (e) q_2 is chosen 59, 60, and 61, respectively. (f) Using one and two via holes, respectively.

4. SIMULATION AND MEASUREMENT RESULTS

The fabricated prototype of the antenna is shown in Fig. 4. The antenna adopts a coaxial port with an SMA connector whose central conductor is connected to the upper patch while its outer conductor is soldered to the ground patch. The measured and simulated reflection coefficients are plotted in Fig. 5, and the results are in good agreement. It is noteworthy that the employment of SMA connector and soldering process can influence the impedance bandwidth especially at 4 GHz. The better match at 4 GHz may result from the soldered tin, which can slow down the input impedance growth. Fig. 6 displays the three-dimensional (3D) radiation patterns of the antenna at 1.8 GHz, 2.4 GHz, and 5.5 GHz, respectively. It can be seen that the gain of the antenna is up to 3.3 dBi at 1.8 GHz, 2.1 dBi at 2.4 GHz, and 4.1 dBi at 5.5 GHz, respectively. In Fig. 7, the details of radiation patterns are plotted at the three resonant frequencies in the x-y, x-z, and y-z observation planes, respectively. Measured and simulated components of the radiation patterns are traced by dashed and solid lines separately. Red and blue lines represent the E_φ and E_θ components of the radiation patterns, respectively. It can be readily observed that the cross-polarization levels in the x-y and x-z planes at 1.8 GHz and 2.4 GHz are very small, and the co-polarization radiation patterns in the x-y and x-z planes are nearly omnidirectional.

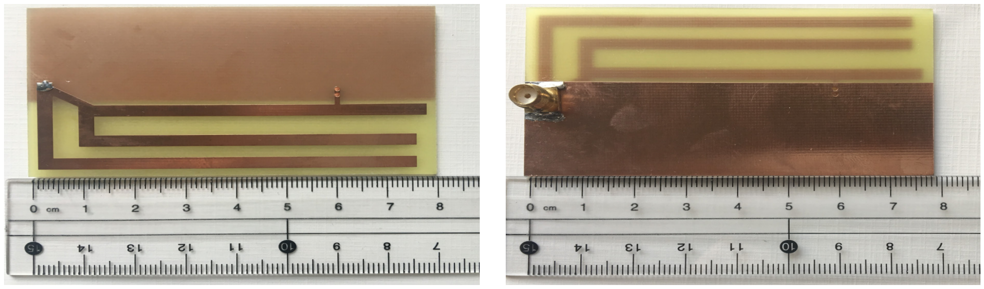

(a) (b)

Figure 4. Fabricated prototype of the proposed antenna. (a) Top view. (b) Bottom view.

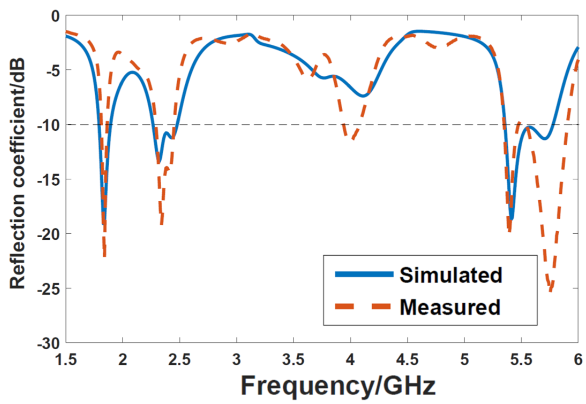

Figure 5. Simulated and measured reflection coefficients versus the frequency.

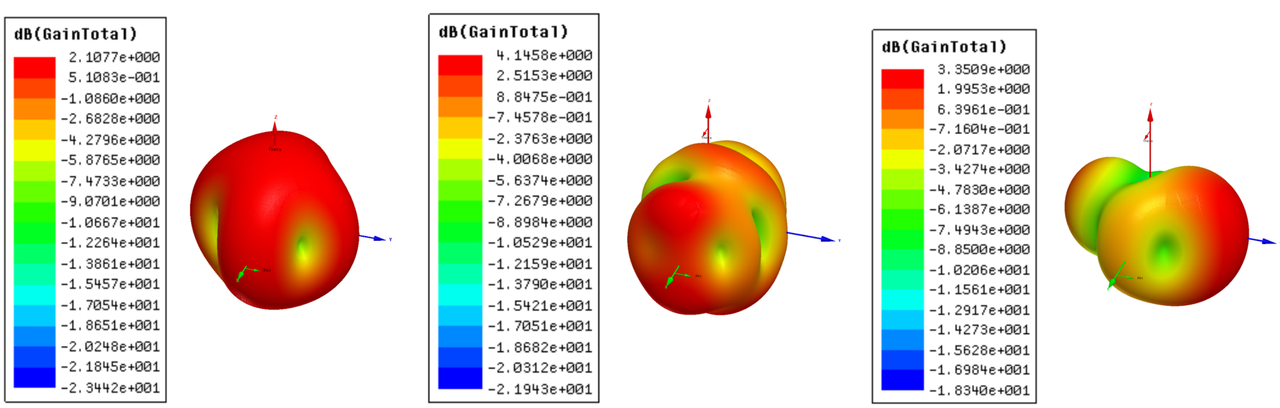

(a) (b) (c)

Figure 6. Three-dimension radiation patterns of the proposed antenna at 1.8 GHz, 2.4 GHz and 5.5 GHz, respectively. (a) 3D radiation pattern at 2.4 GHz. (b) 3D radiation pattern at 5.5 GHz. (c) 3D radiation pattern at 1.8 GHz.

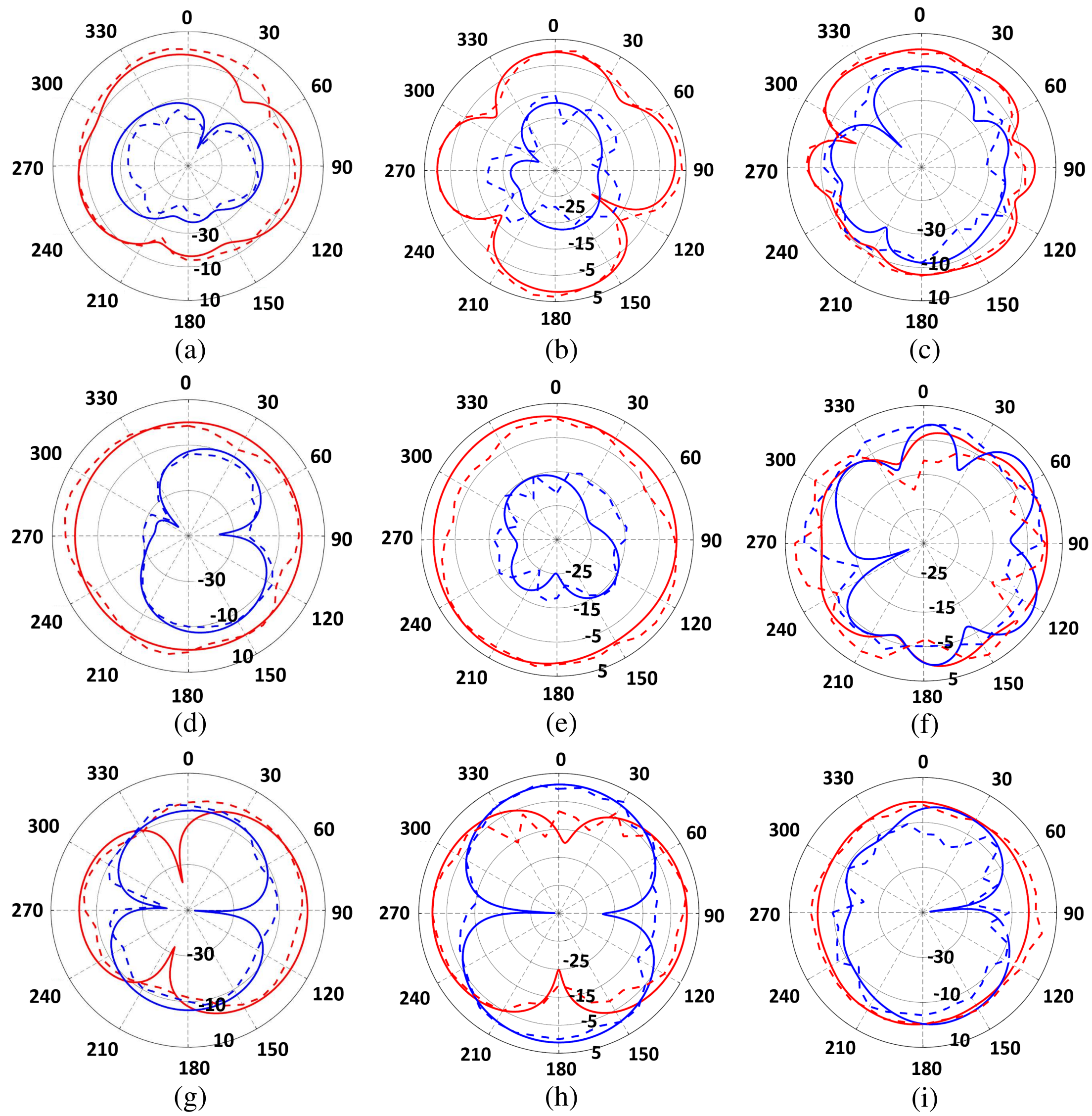

Figure 7. Radiation patterns of the proposed antenna at three resonant frequencies in three observation planes. (a) In the x-y plane at 1.8 GHz. (b) In the x-y plane at 2.4 GHz. (c) In the x-y plane at 5.5 GHz. (d) In the x-z plane at 1.8 GHz.(e) In the x-z plane at 2.4 GHz. (f) In the x-z plane at 5.5 GHz. (g) In the y-z plane at 1.8 GHz. (h) In the y-z plane at 2.4 GHz. (i) In the y-z plane at 5.5 GHz.

The magnitudes of surface current distributions at three resonant frequencies are plotted in Fig. 8. In Fig. 8(a), the segments labeled by 1, 1′, 2, and 2′ all contribute to the radiation pattern at 2.4 GHz because all four segments have a current flow in the x-y plane. In addition, the segments function as dipoles, so the radiation pattern E_φ in the plane is in a four-petal shape, and E_θ is small. The radiation pattern in the x-z plane has a good omnidirectional feature owing to segments 2 and 2′. Because segments 1 and 1′ are located longitudinally in this plane, and the currents in these two segments are out of phase, their contribution to the radiation pattern is insignificant, and the cross-polarization E_θ is weak. In the y-z plane, segments 1 and 1′ contribute to the radiation pattern E_φ. However, due to the opposite phases in the two segments in z-axis, the radiation pattern E_φ decreases significantly. Meanwhile, segments 2 and 2′ contribute to E_θ, and E_θ deviates from that of dipoles when θ is close to 90°. Therefore, the two orthogonally-polarized radiation patterns present an orthogonality in spatiality as shown in Fig. 7(h). Fig. 8(b) shows that when operating at 5.5 GHz, the current distribution of the antenna mainly concentrates on segment 1′, the tilted stub, and the aperture between segment 1′

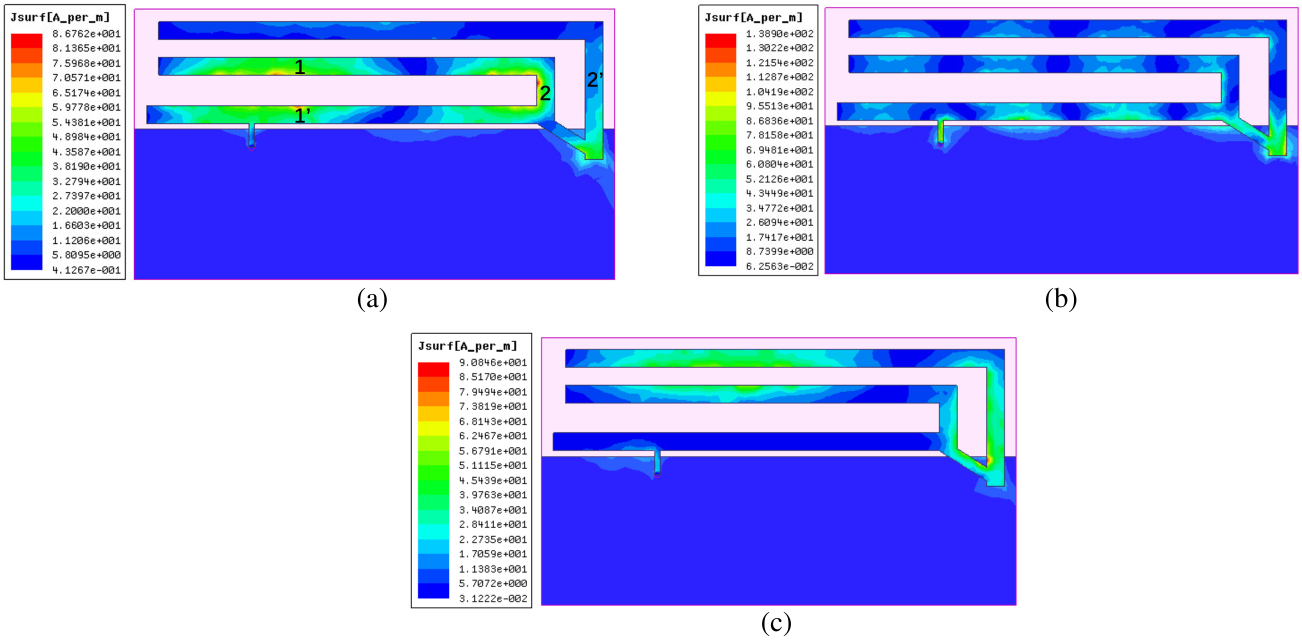

Figure 8. Surface current distributions of the proposed antenna at (a) $f = 2.4\,\text{GHz}$, (b) $f = 5.5\,\text{GHz}$, and (c) $f = 1.8\,\text{GHz}$.

and ground plane. Note that the aperture produces an electric field in it, and the electric field is not vertically polarized owing to the via holes. In addition, according to the relationship $\vec{M}_s = -\hat{n} \times \vec{E}$, the virtual magnetic current will have a vertical component along the aperture. Therefore, the cross-polarization components increase compared with those at 2.4 GHz. Furthermore, the tilted stub will increase the cross-polarization components as well. The higher cross-polarization level is still acceptable for the Wi-Fi and LTE applications in a multi-path signal environment [25]. Fig. 8(c) depicts the current distribution at 1.8 GHz. As explained for the radiation patterns at 2.4 GHz, the radiation patterns at 1.8 GHz are similar to those at 2.4 GHz. However, the co-polarization E_φ in the x-y plane at 1.8 GHz presents a better omnidirectional property due to the strong current from the tilted stub.

The total efficiency of the proposed antenna was measured with the wheeler cap method [26]. The measured and simulated radiation efficiencies versus the frequency are plotted in Fig. 9. The measured radiation efficiencies are roughly 55.0% at 1.8 GHz, 80.0% at 2.4 GHz, and 70.0% at 5.5 GHz, respectively, while the HFSS simulation gives about 56.0%, 85.0%, and 80.0%. It can be seen that the measured and simulated efficiencies are quite close to each other, and the small discrepancy maybe is attributed to the error of adjusting the radius of cylindrical wheeler cap used in the measurement.

Table 2 lists recent designs of triple-band antennas. It is noted that the antennas in [29] and [30] need large grounds which are $150 \times 77\,\text{mm}^2$ and $120 \times 60\,\text{mm}^2$, respectively. It is observed that the proposed antenna in this work has a better comprehensive performance.

Table 2. Comparisons of the proposed antennas with state-of-the-art triple-band PIFA antennas.

	Size (mm^3)	Center freq. (GHz), Relative bandwidth%, Gain (dBi)		
This work	$23 \times 80 \times 1.6$	1.75, 5.46%, 3.3	2.4, 9.7%, 2.1	5.5, 8.4%, 4.1
[27]	$105 \times 70 \times 4.4$	1.8, -, 3.9	2.1, -, 3.37	3.55, -, 8.9
[28]	$40 \times 41 \times 3$	2.21, 18.6%, 2.67	2.89, 30.1%, 1.8	5.58, 23.1%, 7.12
[29]	$32 \times 18 \times 7$	0.89, 4%, -	2.2, 40%, -	3.6, 11%, -
[30]	$12 \times 60 \times 1$	1.575, 1.3%, -0.16	2.4, 8.75%, 2.62	5.8, 31%, 2.04

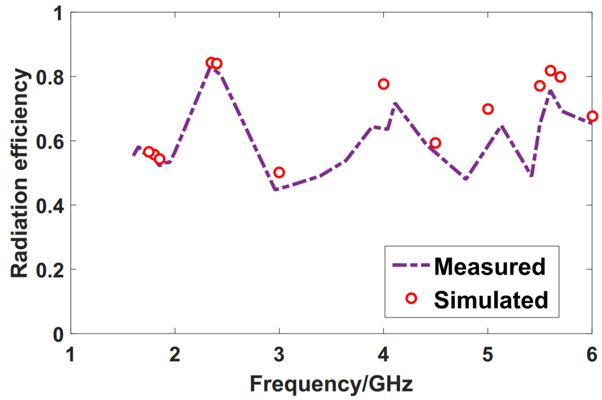

Figure 9. Measured (solid line) and simulated (circle) radiation efficiency against frequency.

5. CONCLUSION

In this work, a compact double PIFA antenna with triple bands is proposed. The antenna has a size of $23 \times 80 \times 1.6\,\mathrm{mm}^3$ and three bands which are suitable for LTE (1.8 GHz) and Wi-Fi (2.4 GHz and 5.5 GHz) applications. The antenna is modified based on the PIFA by adding an extra L-shape open arm to broaden the bandwidth and enhance the gain. The characteristics of the antenna are carefully analyzed, and its performance is optimized in terms of its geometric dimensions for different bands. The prototype of the antenna is manufactured, and its overall performances on impedance bandwidth, radiation patterns, and radiation efficiencies are simulated and measured. The results show that the antenna has a good omnidirectional radiation pattern and the peak gain of 3.3 dBi, 2.1 dBi, and 4.1 dBi, respectively. In addition, the analyses of the functions of arms and via holes provide the guidance of the PIFA design.

REFERENCES

1. Dar, K., M. Bakhouya, J. Gaber, M. Wack, and P. Lorenz, "Wireless communication technologies for ITS applications," *IEEE Commun. Mag.*, Vol. 48, No. 5, 156–162, May 2010.
2. Dardari, D., P. Closas, and P. M. Djuric, "Indoor tracking: Theory, methods, and technologies," *IEEE Trans. Veh. Technol.*, Vol. 64, No. 4, 1263–1278, Apr. 2015.
3. Yang, C. and H. R. Shao, "WiFi-based indoor positioning," *IEEE Commun. Mag.*, Vol. 53, No. 3, 150–157, Mar. 2015.
4. Wu, C., Z. Yang, Z. Zhou, X. Liu, Y. Liu, and J. Cao, "Non-invasive detection of moving and stationary human with WiFi," *IEEE J. Sel. Areas Commun.*, Vol. 33, No. 11, 2329–2342, Nov. 2015.
5. Chen, Z. N., X. M. Qing, T. S. P. See, and W. K. Toh, "Antennas for WiFi connectivity," *Proc. IEEE*, Vol. 100, No. 7, 2322–2329, Jul. 2012.
6. Penttinen, J. T. J., The Telecommunications Handbook, John Wiley & Sons, New Delhi, 2015.
7. Ge, Y., K. P. Esselle, and T. S. Bird, "Compact triple-arm multi-band monopole antenna," *Proc. IEEE Int. Workshop Antenna Technol. (IWAT): Small Antennas Novel Metamaterials*, 172–175, 2006.
8. Su, C. M. and K. L. Wong, "Narrow flat-plate antenna for 2.4 GHz WLAN operation," *Electron. Lett.*, Vol. 39, No. 4, 344–345, Feb. 2003.
9. Wong, K. L., L. C. Chou, and C. M. Su, "Dual-band flat-plate antenna with a shorted parasitic element for laptop application," *IEEE Trans.Antennas Propag.*, Vol. 53, No. 1, 539–544, Jan. 2005.
10. Su, C. M., W. S. Chen, Y. T. Cheng, and K. L. Wong, "Shorted T-shaped monopole antenna for 2.4/5 GHz WLAN operation," *Microwave Opt. Technol. Lett.*, Vol. 41, No. 3, 202–203, May 5, 2004.

11. Liu, D. and B. Gaucher, "A triband antenna for WLAN application," in *Proc. IEEE AP-S Int. Symp. USNC/URSI Nat. Radio Meeting*, Vol. 2, 18–21, 2003.
12. Huitema, L., et al., "Compact and multiband dielectric resonator antenna with pattern diversity for multistandard mobile handheld devices," *IEEE Trans. Antennas Propag.*, Vol. 59, No. 11, 420–428, Nov. 2011.
13. Huang, D. L., H. L. Kuo, C. F. Yang, C. L. Liao, and S. T. Lin, "Compact multibranch inverted-F antenna to be embedded in a laptop computer for LTE/WWAN/IMT-E applications," *IEEE Antennas Wireless Propag. Lett.*, Vol. 9, 838–841, 2010.
14. Franciscatto, B. R., H. Adel, M. H. C. Dias, and T. P. Vuong, "A compact IFA-based dual-band planar antenna for WiFi USB dongles," *Proc. European Conference on Antennas and Propag.*, 325–329, The Hague, 2014.
15. Chiu, C. W. and Y. J. Chi, "Planar hexa-Band inverted-F antenna for portable device applications," *IEEE Antennas and Wireless Propag. Lett.*, Vol. 8, 1099–1102, 2009.
16. Pazin, L., N. Telzhensky, and Y. Leviatan, "Multiband flat-plate inverted-F antenna for Wi-Fi/WiMAX operation," *IEEE Antennas and Wireless Propag. Lett.*, Vol. 7, 197–200, 2008.
17. Wong, K.-L. and C.-Y. Tsai, "Small-size stacked inverted-F antenna with two hybrid shorting strips for the LTE/WWAN tablet device," *IEEE Trans. Antennas Propag.*, Vol. 62, No. 8, 3962–3969, Aug. 2014.
18. Virga, K. and Y. Rahmat-Samii, "Low-profile enhanced-bandwidth PIFA antennas for wireless communications packaging," *IEEE Trans. Microw. Theory Tech.*, Vol. 45, No. 10, 1879–1888, Oct. 1997.
19. Liu, Z. D., P. S. Hall, and D. Wake, "Dual-frequency plannar inverted-F antenna," *IEEE Trans. Antennas Propagat.*, Vol. 45, 1451–1458, Nov. 1997.
20. Salonen, P., M. Keskilammi, and M. Kivikoski, "Single-feed dual-band planar inverted-F antenna with U-shaped slot," *IEEE Trans. Antennas Propag.*, Vol. 48, No. 8, 1262–1264, Aug. 2000.
21. Song, C. T. P., P. S. Hall, P. S. Ghafouri-Shiraz, and D. Wake, "Triple band planar inverted F antennas for handheld devices," *Electron. Lett.*, Vol. 36, No. 2, 112–113, Jan. 2000.
22. Abedin, M. F. and M. Ali, "Modifying the ground plane and its effect on planar inverted-F antennas (PIFAs) for mobile phone handsets," *IEEE Antennas and Wireless Propag. Lett.*, Vol. 2, No. 1, 226–229, 2003.
23. Pazin, L., N. Telzhensky, and Y. Leviatan, "Wideband flat-plate inverted-F laptop antenna for WI-FI/WIMAX operation," *IET Microw. Antennas Propag.*, Vol. 2, No. 6, 568–573, Sep. 2008.
24. Ghosh, S., T. N. Tran, and T. Le-Ngoc, "Miniaturized four-element diversity PIFA," *IEEE Antennas Wireless Propag. Lett.*, Vol. 12, 396–400, 2013.
25. Wang, D. and C. H. Chan, "Multiband antenna for WiFi and WiGig communications," *IEEE Antennas Wireless Propag. Lett.*, Vol. 15, 309–312, 2016.
26. Mendes, C. and C. Peixeiro, "Radiation efficiency of several handset antennas obtained with a modified wheeler cap method," in *Proc. 2nd Eur. Conf. on Antennas and Propagation*, 1–4, 2007.
27. Asadallah, F. A., J. Costantine, and Y. Tawk, "A multiband compact reconfigurable PIFA based on nested slots," *IEEE Antennas Wireless Propaga. Lett.*, Vol. 17, No. 2, 331–334, Feb. 2018.
28. Wakrim, L., S. Ibnyaich, and M. M. Hassani, "Multiband operation and performance enhancement of the PIFA antenna by using particle swarm optimization and overlapping method," *Hindawi Appl. Comput. Intell. Soft Comput.*, 1–8, 2017.
29. Chen, L., Y. Wu, and K. Wong, "Triple-wideband inverted-F frame antenna for the LTE metal-casing smartphone," European Conf. Antennas Propag., 3064–3068, Paris, 2017.
30. Zhang, R., H. Kim, and H. Kim, "Triple-band ground radiation antenna for GPS, WiFi 2.4 and 5 GHz band applications," *Electron. Lett.*, Vol. 51, No. 25, 2082–2084, 2015.